

## Contrasting the Flow Patterns in the Equatorial Pacific Between Two Types of El Niño

Li-Chiao Wang & Chau-Ron Wu

To cite this article: Li-Chiao Wang & Chau-Ron Wu (2013) Contrasting the Flow Patterns in the Equatorial Pacific Between Two Types of El Niño, Atmosphere-Ocean, 51:1, 60-74, DOI: [10.1080/07055900.2012.744294](https://doi.org/10.1080/07055900.2012.744294)

To link to this article: <http://dx.doi.org/10.1080/07055900.2012.744294>



Published online: 21 Nov 2012.



Submit your article to this journal [↗](#)



Article views: 132



View related articles [↗](#)



Citing articles: 2 View citing articles [↗](#)

---

# Contrasting the Flow Patterns in the Equatorial Pacific Between Two Types of El Niño

Li-Chiao Wang and Chau-Ron Wu\*

*Department of Earth Sciences, National Taiwan Normal University, Taipei, Taiwan*

[Original manuscript received 28 September 2011; accepted 12 August 2012]

---

**ABSTRACT** *Outputs based on the National Centers for Environmental Prediction (NCEP) Global Ocean Data Assimilation System (GODAS) are adopted to contrast the current variations in the equatorial Pacific between two types of El Niño. The model fully resolves the equatorial currents. We found that the central Pacific El Niño (CP-El Niño) corresponds well with previous El Niño studies in that both the eastward Equatorial Undercurrent (EUC) and westward South Equatorial Current (SEC) weaken. On the other hand, the eastern Pacific El Niño (EP-El Niño) displays a distinct circulation pattern. The North Equatorial Countercurrent (NECC) strengthens in the developing phase and persists into the peak of the warm event, whereas the northern branch of the SEC (SECn) also intensifies during the mature phase and lasts for about six months. The South Equatorial Countercurrent (SECC) strengthens during the decaying phase of the EP-El Niño. The shifting of the wind stress curl associated with the thermocline variability is chiefly responsible for the unique current performance of the EP-El Niño. It is worth noting that the air–sea interaction plays an important role in the current variability not only during a CP-El Niño but also during an EP-El Niño.*

**RÉSUMÉ** [Traduit par la rédaction] *Nous adoptons les sorties basées sur le système GODAS (Global Ocean Data Assimilation System) des NCEP (National Centers for Environmental Prediction) pour mettre en évidence les variations de courant dans le Pacifique équatorial entre les deux types d'El Niño. Le modèle représente complètement les courants équatoriaux. Nous trouvons que l'El Niño du centre du Pacifique (CP-El Niño) correspond bien aux études précédentes sur l'El Niño puisque le sous-courant équatorial (EUC) vers l'est et le courant sud-équatorial (SEC) vers l'ouest faiblissent. D'autre part, l'El Niño de l'est du Pacifique (EP-El Niño) affiche une configuration de circulation distincte. Le contre-courant nord-équatorial (NECC) se renforce dans la phase de développement et persiste jusqu'au maximum du réchauffement, tandis que la branche nord du SEC (SECn) s'intensifie aussi durant la phase de maturité et persiste pendant environ six mois. Le contre-courant sud-équatorial se renforce durant la phase de dissipation de l'EP-El Niño. Le changement du rotationnel de la tension du vent lié à la variabilité thermocline est principalement responsable du comportement particulier du courant de l'EP-El Niño. Il est à remarquer que l'interaction air–mer joue un rôle important dans la variabilité du courant, non seulement durant un CP-El Niño mais aussi durant un EP-El Niño.*

**KEYWORDS** EP-El Niño; CP-El Niño; Equatorial Pacific currents; wind stress curl

---

## 1 Introduction

The significance of ocean–atmosphere interactions in the tropical Pacific Ocean has been recognized and documented (e.g., Bjerknes, 1969; Philander, Yamagata, & Pacanowski, 1984). Understanding the dynamics of the equatorial Pacific Ocean is essential to the global climate. The seasonal cycle is one of the predominant fluctuations in the region (Yu & McPhaden, 1999), resulting ultimately from solar radiation and the coupled air–sea–land interaction (Li & Philander, 1996). Beyond the seasonal time scale, the climate variability demonstrates an interannual variation related to the El Niño–Southern Oscillation (ENSO) (e.g., Philander, 1990). Because the variability of atmospheric anomalies is sensitive to variations in sea surface temperature (SST), the description

of ENSO in previous studies is often based on SST variability, which has been studied extensively. However, the equatorial currents and the processes that modulate their circulation patterns have not been discussed as extensively because of the lack of measurements in the region. The variability of the equatorial current is not well understood at interannual or longer time scales, and the dynamics involved is worth further investigation. The current fluctuations in the region are largely influenced by atmospheric conditions, which in turn are modulated by the ENSO phenomenon.

Among the studies of the tropical Pacific Ocean circulation, there are only a few capable of providing sufficient data to describe the mean flow pattern from contemporaneous observations. For example, Yu and McPhaden (1999) described the

---

\*Corresponding author's email: cwu@ntnu.edu.tw

## Equatorial Pacific Currents during Two Types of El Niño / 61

Table 1. Classification of the El Niño events.

	Canonical type	New type	The third type (cannot be classified yet)
El Niño Modoki Ashok et al. (2007)	<i>Canonical El Niño</i> SSTA: warm in the eastern Pacific; with eastward Kelvin waves Years: The other events.	<i>El Niño Modoki</i> SSTA: warm in the central Pacific; without eastward Kelvin waves Years: 1979/80, 1986/87, 1990/91, 1991/92, 1992/93, 1994/95, 2002/03, 2004/05	
EP- and CP-El Niño Kao and Yu (2009)	<i>EP- El Niño</i> SSTA: warm in the eastern Pacific associated with thermocline variations, surface winds Years: 1972/73, 1976/77, 1982/83, 1997/98	<i>CP- El Niño</i> SSTA: warm in the central Pacific influenced by the atmospheric forcing Years: 1991/92, 1994/95, 2002/03, 2004/05, 2006/07	
CT and WP El Niño Kug et al. (2009)	<i>CT El Niño</i> SSTA: warm in the Niño-3 (5°S–5°N, 90°W–150°W) Years: 1972/73, 1976/77, 1982/83, 1997/98	<i>WP El Niño</i> SSTA: warm in the Niño-4 (5°S–5°N, 150°W–160°E) Years: 1977/78, 1990/91, 1994/95, 2002/03, 2004/05	<i>The third type</i> SSTA: warm in Niño-3.4 (5°S–5°N, 120°W–170°E) Years: 1986/87, 1987/88, 1991/92

annual cycle of zonal currents along the equator based on the Tropical Ocean Global Atmosphere (TOGA) Tropical Atmosphere Ocean (TAO) project array. In the western Pacific Ocean, hydrographic sections and Acoustic Doppler Current Profiler (ADCP) observations collected between 1984 and 1991 were used in a dynamical interpretation of the mean circulation (Gouriou & Toole, 1993). The termination of the Equatorial Undercurrent (EUC) has been examined with historical hydrographic data in the eastern Pacific Ocean (Lukas, 1986). Although these measurements have shed some light on the mean circulation in the region, much less is known about the interannual variability related to ENSO. Two pioneering studies found that the currents in the equatorial Pacific Ocean are considerably altered during ENSO events. Using hydrographic sections and ADCP data, Delcroix, Eldin, Radenac, Toole, and Firing (1992) documented current variations during the 1986/87 El Niño and the subsequent La Niña. The same sections were further examined by Johnson, Mcphaden, Rowe, and McTaggart (2000) to investigate the equatorial flow fluctuation during the 1997/98 El Niño.

Complex features of the evolution of ENSO have recently been recognized and studied. These studies suggest that there are two different types of El Niño (Ashok, Behera, Rao, Weng, & Yamagata, 2007; Kao & Yu, 2009; Kug, Jin, & An, 2009; Yeh et al., 2009). Table 1 summarizes the characteristics and classifications of the El Niño events. In Table 1, the definition of El Niño Modoki is based on the location of the SST anomalies (Ashok et al., 2007). During El Niño Modoki, SST anomalies appear to be associated with a horseshoe pattern in the central Pacific Ocean. The monthly indices and anomaly fields are seasonally averaged over the period from June to September (December to February) as the boreal summer (winter) values. Kao and Yu (2009) pointed

out that during the eastern Pacific El Niño (EP-El Niño), SST anomalies emerge from the coast of South America, propagate westward to the central Pacific Ocean and decay off the equator. In the central Pacific El Niño (CP-El Niño), SST anomalies first appear around the date line, develop and mature into a V-shaped anomaly structure extending toward the subtropics in both hemispheres and then decay in the equatorial central Pacific Ocean. Kug et al. (2009) found and defined the cold tongue (CT) El Niño; it has a pattern of large SST anomalies in the eastern Pacific Ocean during the summer. The maximum value of the warm SSTs is located in the coastal region of the eastern boundary. The SST anomalies of the warm pool (WP) El Niño are mostly confined to the central Pacific Ocean during the boreal summer. A broad seasonal mean from September to the following February is taken to classify the El Niño events.

In this study, we follow the definition and methodology of Kao and Yu (2009). The canonical El Niño is significant in EP-El Niño. This new type of El Niño, which is different from the canonical El Niño in both the location of the maximum SST anomalies and its tropical mid-latitude teleconnections, is the CP-El Niño. The two types of El Niño have their own evolution processes and thermocline structures, bringing distinct modulations to the ocean currents.

To have a better description of the equatorial current pattern on the ENSO time scale, the analyses have to contrast current patterns of the two types of El Niño. The limited measurements in the equatorial Pacific Ocean are not suitable for the longer time scale study. In this study, we use an ocean model product to investigate the equatorial current variability and the way it is associated with the different types of El Niño. The paper is structured as follows. In Section 2 we describe the dataset used in this study. In Section 3, spatial and temporal variations of assimilated equatorial currents using the dataset

are presented. The distinct evolution patterns of the currents associated with a CP-El Niño and an EP-El Niño and their forcing mechanisms are also described. Section 4 concludes this paper.

## 2 Data

The current velocity and 20°C isotherm depth anomaly data used in this study are based on the National Centers for Environmental Prediction (NCEP) Global Ocean Data Assimilation System (GODAS) product (Behringer & Xue, 2004). The GODAS domain extends from 75°S to 65°N with a horizontal resolution of  $1/3^\circ \times 1/3^\circ$ . The model has 40 levels with 10 m resolution near the sea surface and is forced by momentum, heat and freshwater flux from the NCEP atmospheric reanalysis 2 (R2) (Kanamitsu et al., 2002). The temperature profiles assimilated in GODAS include those from the TOGA experiment TAO, the Prediction and Research Moored Array in the Atlantic (PIRATA) project, the Triangle Trans-Ocean Buoy Network (TRITON) moorings, expendable bathythermographs (XBTs), and Argo profiling floats. In addition to temperature, a synthetic salinity profile is computed for each temperature profile using a local *T-S* climatology based on annual mean fields of temperature and salinity from the National Oceanic Data Center (NODC) World Ocean Database.

Surface wind stress data back to 1948 are provided by the NCEP/National Center for Atmospheric Research (NCAR) reanalysis project. Monthly averages on global grids ( $2.5^\circ \times 2.5^\circ$ ) are available from the Climate Diagnostics Center of the Earth System Research Laboratory, National Oceanic and Atmospheric Administration (NOAA) (<http://www.cdc.noaa.gov/>).

## 3 Results and discussion

### a *The Equatorial Currents*

The assimilated mean circulation pattern for the Pacific equatorial current is plotted in Fig. 1a, which is consistent with the observational mean flow pattern in the region (e.g., Lukas, 2001). The equatorial zonal currents consist of a westward-flowing wide-range surface current, the South Equatorial Current (SEC), which is located between about 8°S and 3°N. Following the definition of Wyrtki (1974), the SEC is further split into northern and southern branches by the equator, hereafter called the SEC<sub>n</sub> and SEC<sub>s</sub>, respectively. To the north, the eastward-flowing current is the North Equatorial Countercurrent (NECC; between about 5°N and 10°N). North of the NECC, there is an intense westward current, the North Equatorial Current (NEC; between about 10°N and 20°N). The NEC is the southern limb of the North Pacific subtropical gyre and is upstream of the Kuroshio. The South Equatorial Countercurrent (SECC) extends eastward from the western boundary region, but it only reaches the central and eastern Pacific intermittently.

A vertical profile along the equator averaged from approximately 2°N to 2°S using GODAS data is shown in Fig. 1b. The most prominent currents here are the subsurface eastward EUC (red shading) and the westward SEC (blue shading). The EUC is the strongest equatorial current that travels across the Pacific. It originates at about 140°E, strengthens and reaches its maximum speed between 155°W and 125°W and weakens considerably east of 90°W. The assimilated results from GODAS agree well with observations (Johnson, Sloyan, Kessler, & McTaggart, 2002; Yu & McPhaden, 1999). Furthermore, the core of the EUC gets closer to the sea surface as it flows eastward, which in turn feeds the equatorial upwelling. This shoaling process largely influences the SST in the eastern Pacific Ocean, where the air–sea interaction is important. As a result, the EUC plays an important role in both seasonal and interannual fluctuations around the equatorial region (Gu & Philander, 1997), as well as in the climate response to global warming (Cai & Whetton, 2000). The strong EUC prevails at depths up to 400 m, while the relatively weaker SEC is limited to the upper 50 m. The GODAS result is very similar to the velocity profile plotted by Lukas (2001) based on the ocean assimilation/reanalysis product from NOAA/NCEP.

Figures 2a to 2c show the annual cycle of zonal currents on the equator at 165°E, 140°W and 110°W, respectively. The sections have previously been used to describe the annual cycle of the equatorial currents (Yu & McPhaden, 1999). Following Keenlyside and Kleeman (2002), the annual cycle is described in terms of velocity anomalies (i.e., with climatology removed). The structures of the annual cycle at all three locations are similar. There is an eastward intensification of the currents, occurring between March and July, which extends from the surface to the depth of the EUC. At 165°E, the EUC is strongest in July, and the depth of the core is located at about 60–150 m (Fig. 2a). At 140°W, the EUC core is located at 60 m depth, and the fastest flow occurs in May (Fig. 2b). At 110°W, the EUC is strongest during April and May, and the core shoals to approximately 25 m (Fig. 2c). These annual cycle patterns agree well with those from the TAO array data, except for a slight discrepancy in the magnitude of the current velocity (Figs 2d to 2f; Keenlyside & Kleeman, 2002).

### b *Spatial Variations Associated with the CP- and EP-El Niño*

The modulation of the equatorial currents by the two types of El Niños is now investigated. Figure 3 shows meridional velocity profiles along 140°W in the boreal winter, including the composited normal year, CP-El Niño and EP-El Niño. We averaged from December to February of the following year, defined as the boreal winter, which was identified as the mature phase of El Niño by Kug et al. (2009, Kug, Choi, An, Jin, & Wittenberg, 2010). In the boreal winter of normal years, eastward currents include the EUC and NECC (Fig. 3a). The EUC is located in the thermocline from 20 m to 300 m and its core is near 140 m. It is trapped in the equatorial

## Equatorial Pacific Currents during Two Types of El Niño / 63

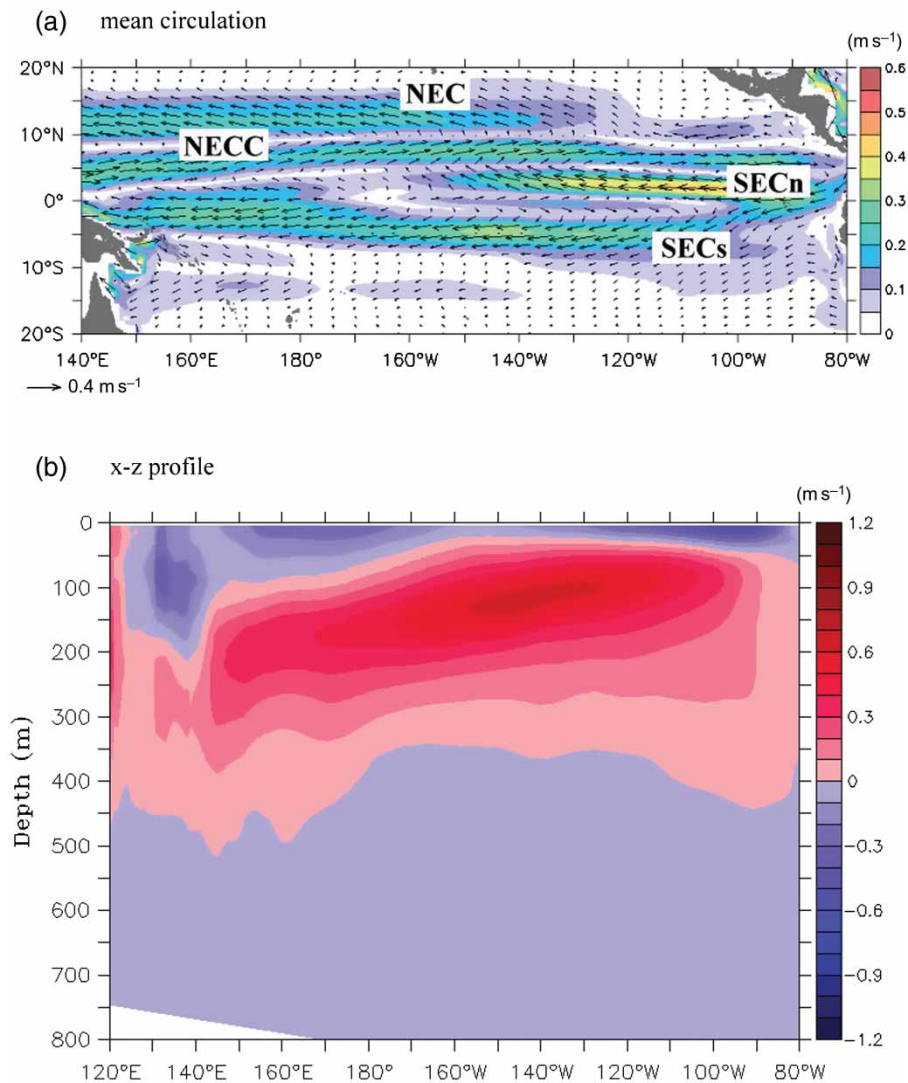


Fig. 1 (a) Mean surface circulation (averaged from 0 to 50 m) in the equatorial Pacific Ocean based on GODAS model assimilation (units are  $\text{m s}^{-1}$ ). The shading indicates the current intensity. The contour interval is  $0.05 \text{ m s}^{-1}$ . (b) Vertical velocity profile along the equator averaged from approximately  $2^\circ\text{N}$  to  $2^\circ\text{S}$  from the assimilated annual mean (units are  $\text{m s}^{-1}$ ). The contour interval is  $0.1 \text{ m s}^{-1}$ . Red and blue shading indicate the eastward and westward current, respectively.

region between  $2^\circ\text{S}$  and  $2^\circ\text{N}$ . The NECC, centred at  $7^\circ\text{N}$ , has its maximum velocity near 50 m depth. Westward currents include the SECn, SECs and NEC. The SECn is present at approximately  $3^\circ\text{N}$  and is strongest in the central Pacific between  $90^\circ\text{W}$  and  $140^\circ\text{W}$ . The SECs, centred at approximately  $5^\circ\text{S}$ , is relatively weaker at  $140^\circ\text{W}$  but has a wider range than that of the SECn. The NEC is located between  $10^\circ\text{N}$  and  $20^\circ\text{N}$  and is very weak at  $140^\circ\text{W}$ .

During a CP-El Niño winter, the EUC is significantly weakened near its core (Fig. 3b). The SECn becomes weaker and narrower, probably because of the weakening easterly trade winds at the equator (Johnson et al., 2002). On the other hand, the SECs becomes a little stronger than in a normal year at  $140^\circ\text{W}$ . The NEC is also stronger during a CP-El Niño than during a normal year. The flow patterns during a CP-El Niño agree well with previous El Niño studies (e.g.,

Johnson et al., 2002; Keenlyside & Kleeman, 2002; Lukas, 2001; Yu & McPhaden, 1999).

The velocity profile during the EP-El Niño (Fig. 3c) mature phase is significantly different from that during a CP-El Niño. The westward SECn, which weakens during a CP-El Niño compared with those in normal years, merges with the SECs and strengthens at  $140^\circ\text{W}$  during an EP-El Niño. The eastward EUC weakens and descends to more than 600 m depth, probably as a result of the depression from the strong SEC. This feature is not consistent with the earlier finding that the EUC disappeared during the 1997/98 El Niño (e.g., Johnson et al., 2002). We suggest that the EUC still exists but is depressed and descends to a lower depth because of the intensification of the SEC during an EP-El Niño. A similar pattern is seen in other ocean data assimilation models, such as the Simple Ocean Data Assimilation (SODA) Parallel Ocean

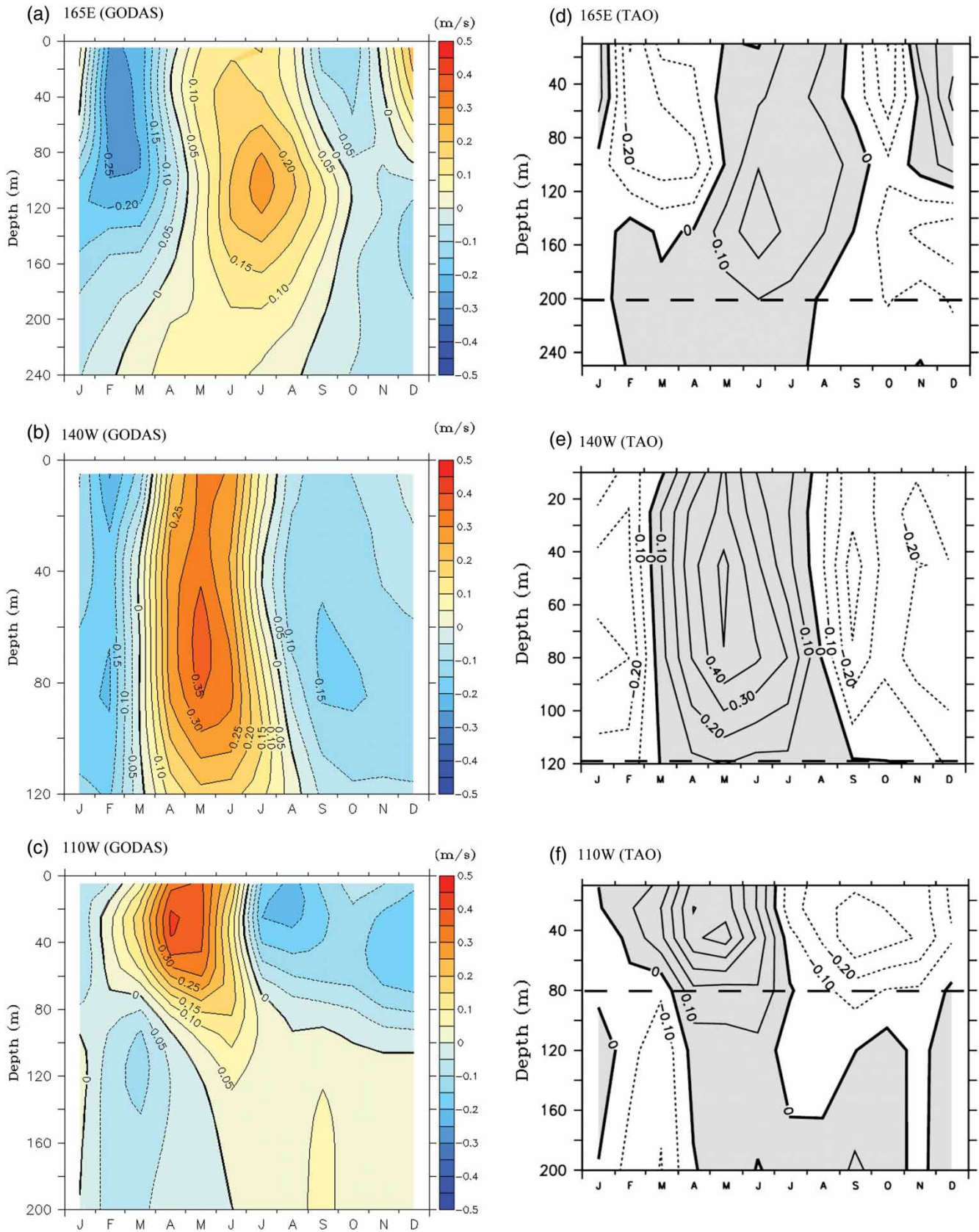


Fig. 2 The annual cycle of zonal currents on the equator from the model assimilation at (a) 165°E, (b) 140°W and (c) 110°W, respectively (units are  $m s^{-1}$ ). (d) to (f) are the same as (a) to (c), but are based on TAO array data (adapted from Fig. 2 of Keenlyside & Kleeman, 2002 by permission of the American Geophysical Union). The contour interval is  $0.05 m s^{-1}$ .

### Equatorial Pacific Currents during Two Types of El Niño / 65

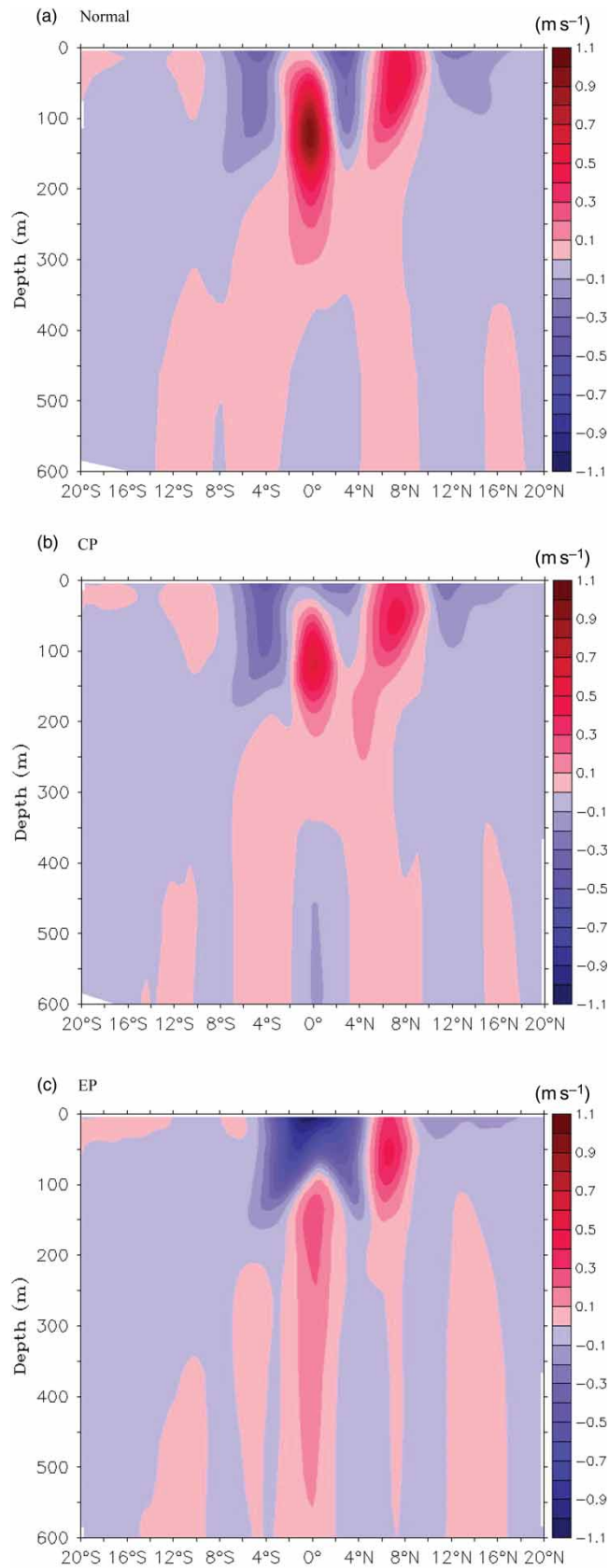


Fig. 3 Composit ed meridional velocity profiles from GODAS along 140°W in winter of (a) normal years, (b) CP-El Niño, (c) EP-El Niño. Red and blue shading indicate the eastward and westward current (units are  $\text{m s}^{-1}$ ). The contour interval is 0.1  $\text{m s}^{-1}$ .

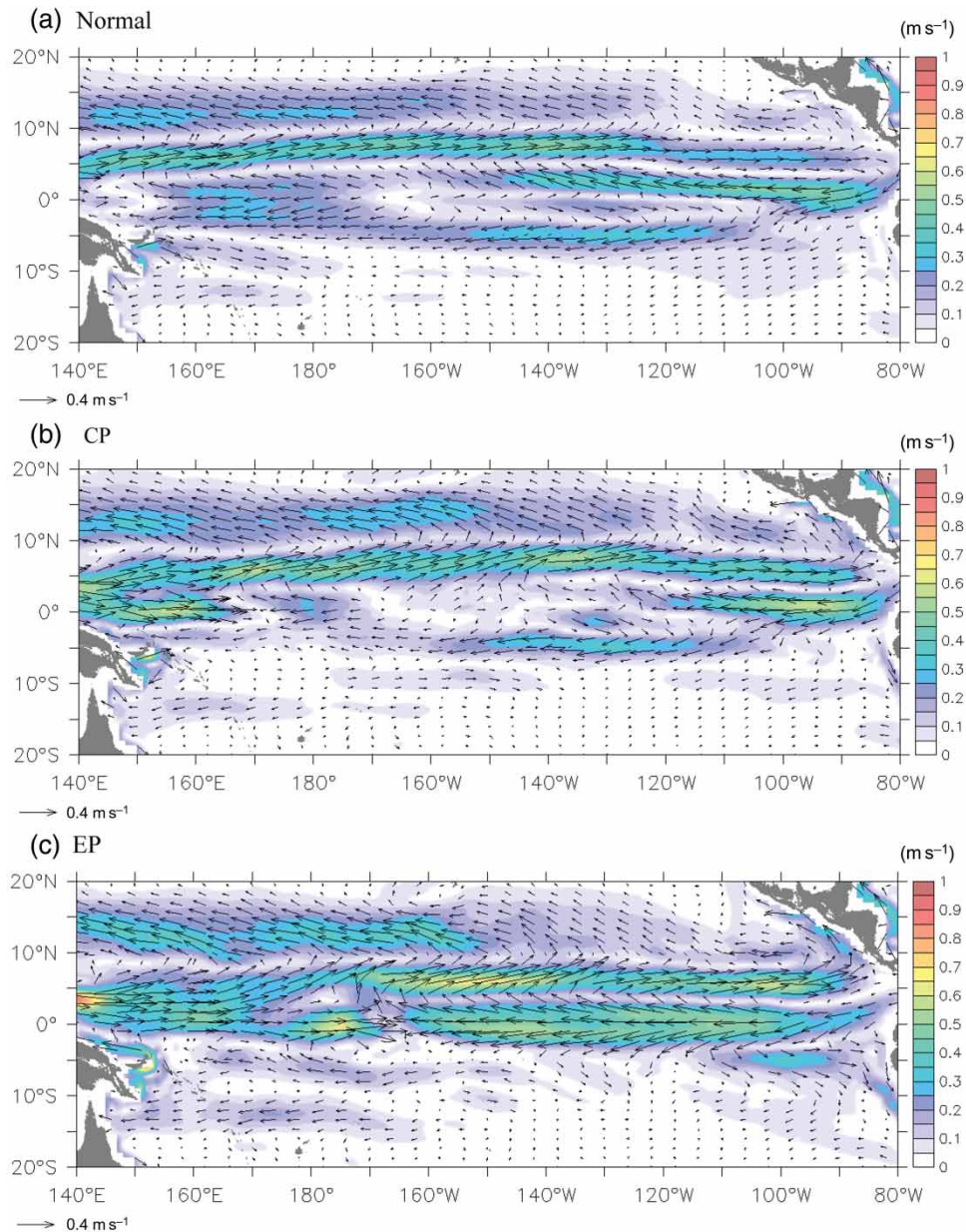


Fig. 4 As in Fig. 1a, but for winter of (a) normal years, (b) CP-El Niño, (c) EP-El Niño.

Program (POP), version 1.4.2, and the Geophysical Fluid Dynamics Laboratory (GFDL) Coupled Model Assimilation (figures not shown).

A composite of the spatial circulation patterns in the equatorial Pacific Ocean for the normal, CP-El Niño and EP-El Niño winters are plotted in Fig. 4. During a normal winter, the SECn and SECs are obviously separated from each other. The SECn persists until the dateline and extends westward intermittently thereafter, whereas the SECs seems to be capable of reaching the western Pacific basin (Fig. 4a). The eastward NECC located between 4°N and 9°N, and the subsurface current EUC, is not obvious at 50 m depth. However, in the mature phase of a CP-El Niño, the NECC

strengthens and the EUC shoals up to the sea surface west of 170°E (Fig. 4b). The SECn becomes much weaker and is confined east of 120°W. The SECs is blocked by the shoaling EUC and is not able to reach the western boundary.

The circulation during an EP-El Niño has a distinctive pattern. Most of the previous studies indicate that the EUC obviously weakens as it flows eastward during an El Niño. In this study, we found that these earlier findings are valid only during a CP type of El Niño. The EUC strengthens from the onset till the mature phase of an EP-El Niño (figure not shown) and merges with the NECC, surging eastward. This unusual performance of the eastward currents is supposed to be a great disturbance in the westward currents.

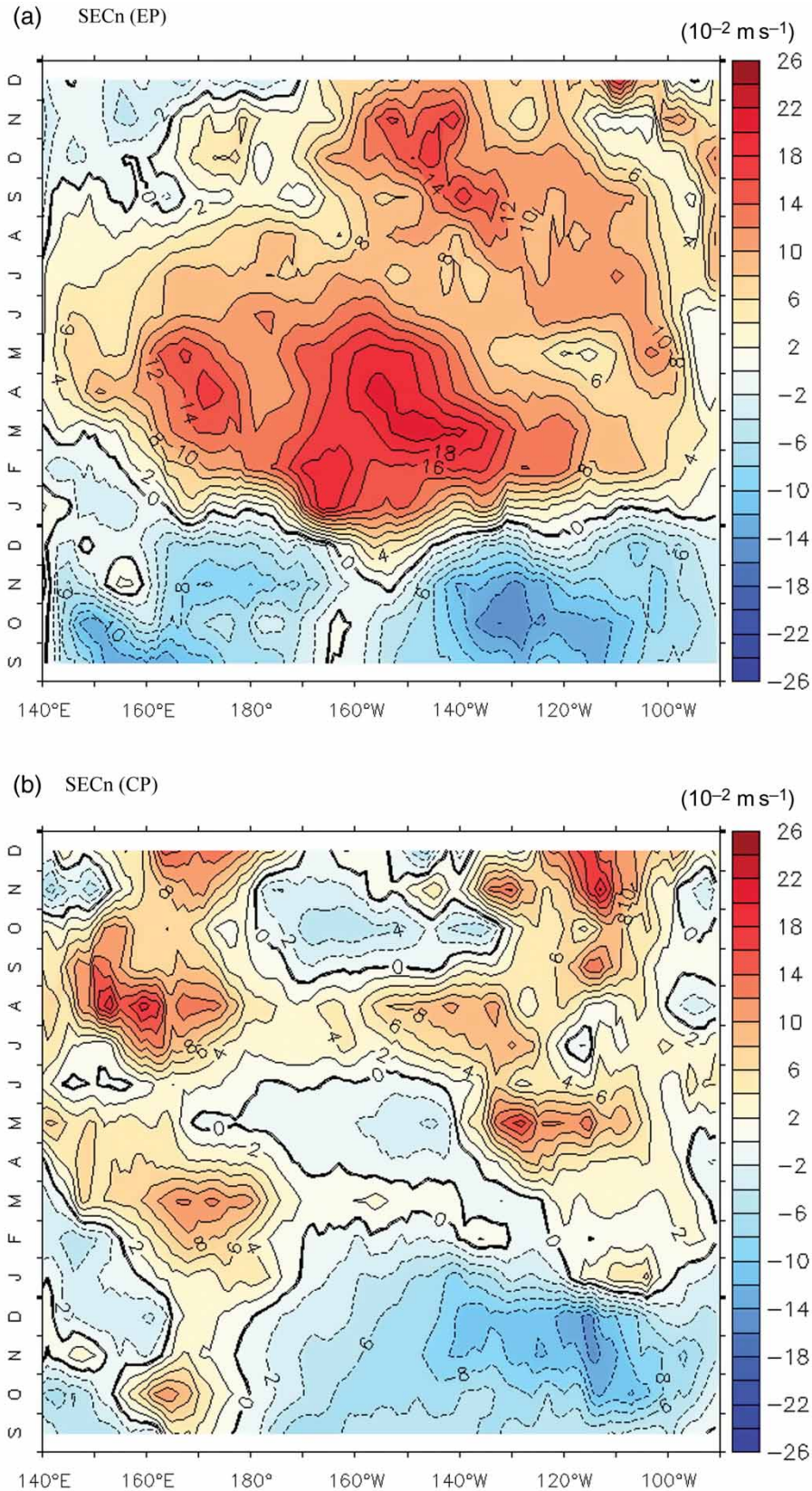


Fig. 5 Compositing velocity anomalies of SECn during the evolution of El Niño. In (a) the EP-El Niño and (b) the CP-El Niño. Positive values (red shading) indicate westward anomalies, whereas negative values (blue shading) indicate eastward anomalies. The data are averaged over the region 0 to 7°N approximately, and depths from 0 to 300 m. The contour interval is 0.02 m s<sup>-1</sup>.

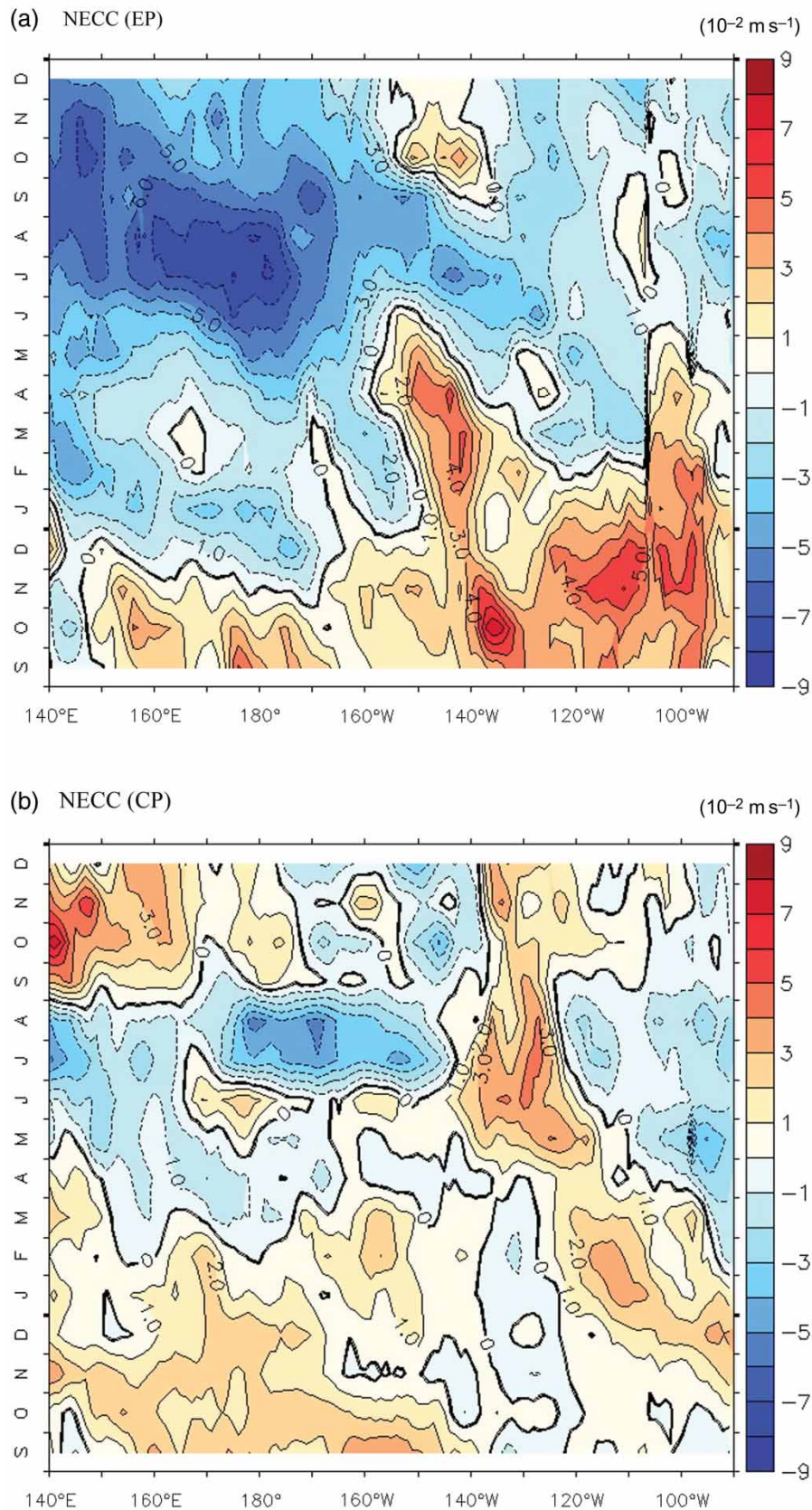


Fig. 6 As in Fig. 5 except for the NECC. Positive values (red shading) indicate eastward anomalies, and negative values (blue shading) indicate westward anomalies. The data are averaged over the region  $3.5^{\circ}\text{N}$ – $10^{\circ}\text{N}$  approximately and depths from 0 to 500 m. The contour interval is  $0.01 \text{ m s}^{-1}$ .

## Equatorial Pacific Currents during Two Types of El Niño / 69

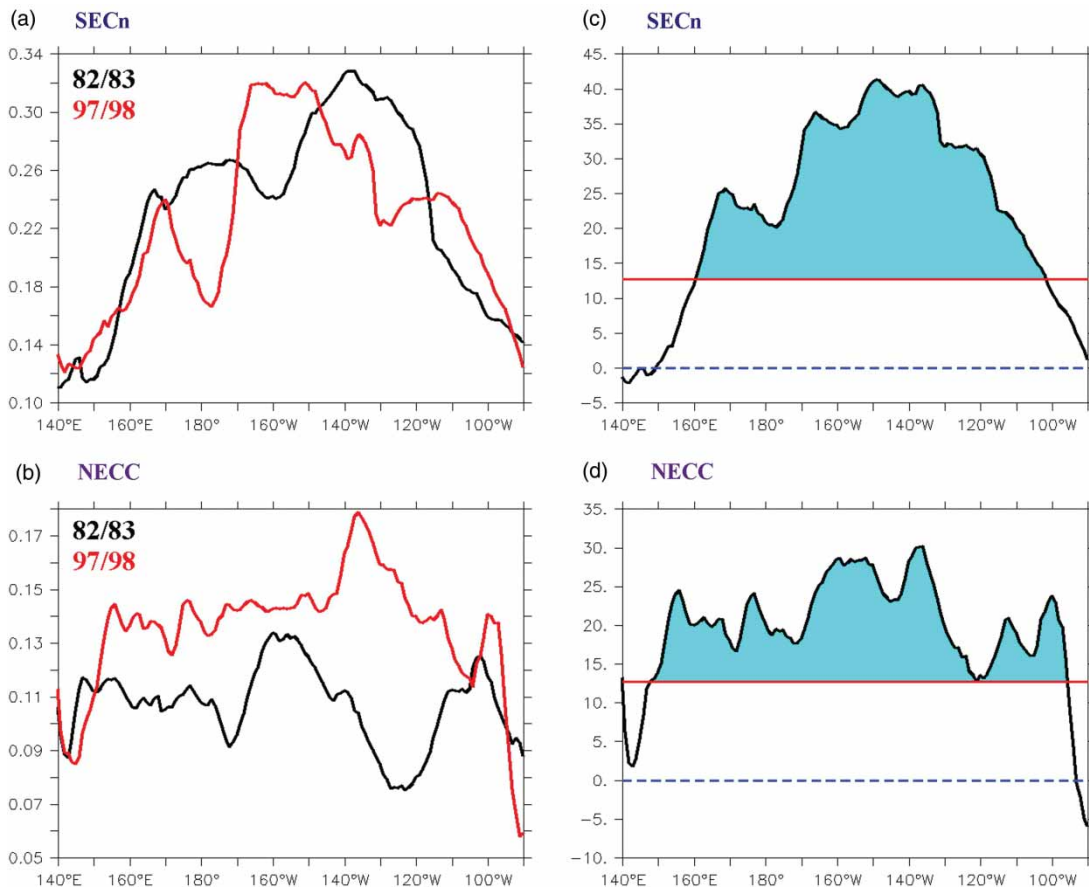


Fig. 7 Velocity intensity pattern of (a) the SECn during the mature phase together with (b) the NECC during the developing phase of the two EP El Niño events. The black line indicates the 1982/83 event, and the red line indicates the 1997/98 event (units are  $\text{m s}^{-1}$ ). (c) and (d) show the  $t$  value of the SECn and NECC during the composited EP-El Niño (black line). The red line denotes the 95% confidence level. The light-blue colour highlights the significant zone.

However, the SECn and SECs also merge and strengthen. These two merged current systems being in opposite directions and equally strong, counteract each other around  $170^\circ\text{W}$ . This unusual pattern appears only during an EP-El Niño and is far from what has been discussed in earlier El Niño studies. The strengthening region of the eastward EUC during the mature phase of an EP-El Niño is confined to west of the dateline, whereas it weakens significantly east of the dateline, where the merged SECn and SECs is exceptionally vigorous. The intense westward currents suppress the eastward EUC and NECC around the equator, which produces an unusual flow pattern during an EP-El Niño (Fig. 4c). Moreover, it is often observed that the NEC tends to migrate northward as it flows westward during an El Niño. Figure 4c shows that the NEC is at approximately  $16^\circ\text{N}$  latitude when it reaches the western Pacific Ocean boundary. The bifurcation point of the NEC is much farther north during an EP-El Niño than during a CP-El Niño.

### c Temporal Variations of the Equatorial Currents

To place emphasis on the interannual variability, we remove the annual cycle signal and deal with the velocity anomalies in the subsequent analysis. We identified the phases of El Niño

evolution according to Kug et al. (2009, 2010). The developing phase occurs from March to November, the mature phase from December to February of the following year, and the decay phase from February to October. Figures 5 and 6 present composites of the velocity anomalies of the main equatorial currents during the evolution of an EP-El Niño and a CP-El Niño. For the westward SECn, positive values (red shading) indicate westward anomalies, and negative values (blue shading) indicate eastward anomalies. The westward SECn weakens during the onset of an EP-El Niño. Immediately after the mature phase, the SECn strengthens and reaches its maximum in the central Pacific Ocean around  $140^\circ\text{W}$ – $170^\circ\text{W}$  (Fig. 5a). The strengthening of the SECn persists into the following year. During a CP-El Niño, the SECn tends to be weakened (Fig. 5b), which is in agreement with the behaviour of the SECn observed in previous El Niño studies (e.g., Johnson et al., 2002). The SECn during a CP-El Niño is generally weaker in the central Pacific Ocean. Though it seems to recover for a time in the western Pacific Ocean, its intensity is still weak compared with the strong and continuous SECn during an EP-El Niño.

Figure 6 presents the velocity anomalies of the evolution of the NECC. For the eastward NECC, positive values (red shading) indicate eastward anomalies, and negative values

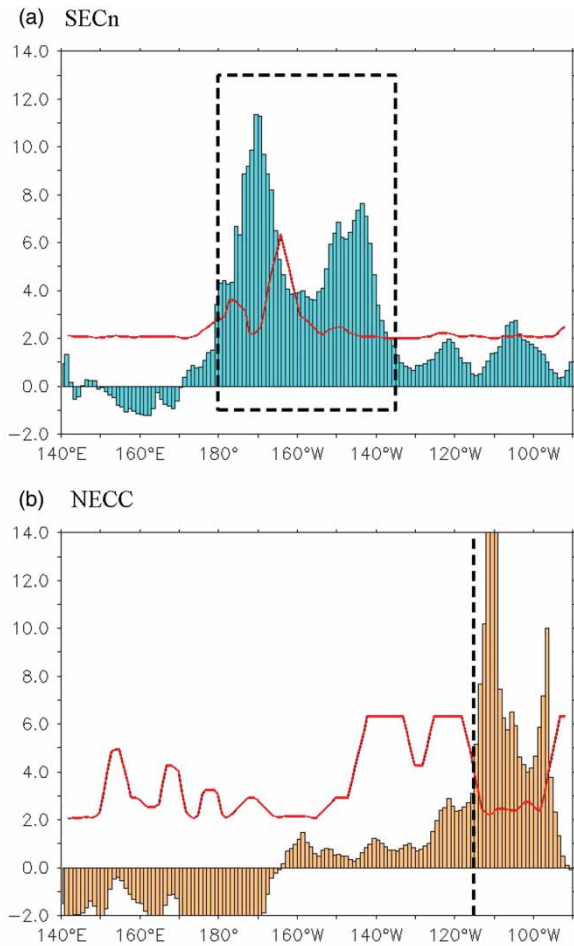


Fig. 8 Statistical  $t$  value (bars) between EP-El Niño and CP-El Niño for (a) the SECn during the mature phase and (b) the NECC during the developing phase. The red curve denotes the 90% confidence level.

(blue shading) indicate westward anomalies. During an EP-El Niño, the NECC strengthens across the entire Pacific basin, and the surge in the eastern Pacific Ocean is particularly conspicuous (Fig. 6a). The eastward surface NECC is reinforced immediately after leaving the western boundary, with much more intensification taking place to the east of  $150^{\circ}\text{W}$ . The strengthening persists for several months into the mature warm phase. Compared with the EP type of El Niño, the CP-El Niño usually behaves close to the seasonal climatology (Fig. 6b).

A statistical significance check was carried out to demonstrate that the composite analysis (for EP-El Niño events) is representative of the EP type of El Niño. The composite result is investigated statistically using the one-sample  $t$ -test

$$t = \frac{\bar{x} - \mu}{\text{SD}_{\bar{x}}}$$

where  $\bar{x}$  is the variable considered,  $\mu$  is the mean, and SD is the standard error at the 95% confidence level. Figures 7a and 7b show the velocity pattern (absolute value, for clarity) of the

SECn and the NECC during the two EP-El Niño events. The 1982/83 event (black line) and the 1997/98 event (red line) behave similarly except that the NECC intensity of the 1997/98 event is larger than that of the 1982/83 event (Fig. 7b), and the longitude of the maximum velocity differs slightly. Figures 7c and 7d show the  $t$  value of zonal currents during the EP-El Niño. The red lines denote the 95% confidence level, and the significance zone is highlighted in blue. During the EP-El Niño, the significance zone for the SECn is from approximately  $105^{\circ}\text{W}$  to  $160^{\circ}\text{E}$ , and the significance zone for the NECC is from approximately  $95^{\circ}\text{W}$  to  $150^{\circ}\text{E}$ . The range mentioned in Figs 5 and 6 falls into this significance zone, indicating that the composite result of the EP-El Niño is meaningful. A similar statistical significance check was done for the CP-El Niño, and its composite result is also significant (figure not shown).

Moreover, a Welch  $t$ -test (Welch, 1947) was used to assess the significance of the difference between means of current velocities during the EP-El Niño and the CP-El Niño. Unlike the Student's  $t$ -test that is based on a pooled variance estimate, the Welch  $t$ -test compares variables of unequal size and variance. The statistical  $t$  value to test whether the means are different or not can be calculated as

$$t = \frac{\bar{X}_1 - \bar{X}_2}{S_{\bar{X}_1 - \bar{X}_2}},$$

where

$$S_{\bar{X}_1 - \bar{X}_2} = \sqrt{\frac{s_1^2}{n_1} + \frac{s_2^2}{n_2}},$$

and  $\bar{X}_1$ ,  $\bar{X}_2$  represent the means of the EP-El Niño and the CP-El Niño, respectively;  $S$  is the variance;  $s_1$  and  $s_2$  represent the variance of EP-El Niño and CP-El Niño, respectively;  $n_1$  and  $n_2$  are the sample sizes. The degree of freedom (df) was calculated using the Welch-Satterthwaite equation:

$$\text{df} = \frac{(s_1^2/n_1 + s_2^2/n_2)^2}{(s_1^2/n_1)^2/(n_1 - 1) + (s_2^2/n_2)^2/(n_2 - 1)}.$$

Figure 8 shows the  $t$  value (bars) of the velocity anomalies of the zonal currents. Based on the red curve which indicates the 90% confidence level, the SECn is strong from  $180^{\circ}\text{E}$  to  $140^{\circ}\text{W}$  during the EP-El Niño (Fig. 8a). The area covers most of the strengthening region described in Fig. 5. Similarly, the NECC is strong in the eastern Pacific Ocean, especially east of  $120^{\circ}\text{W}$  during the EP-El Niño (Fig. 8b). It seems to be smaller than that mentioned in Fig. 6, probably because of the spatial difference of the NECC's intensification between the 1982/83 and 1997/98 El Niño events (see Fig. 7b). It still captures the major strengthening pattern of the NECC during the EP-El Niño compared to the CP-El Niño. The region where the zonal currents are significantly different between the two types of El Niño events matches the

## Equatorial Pacific Currents during Two Types of El Niño / 71

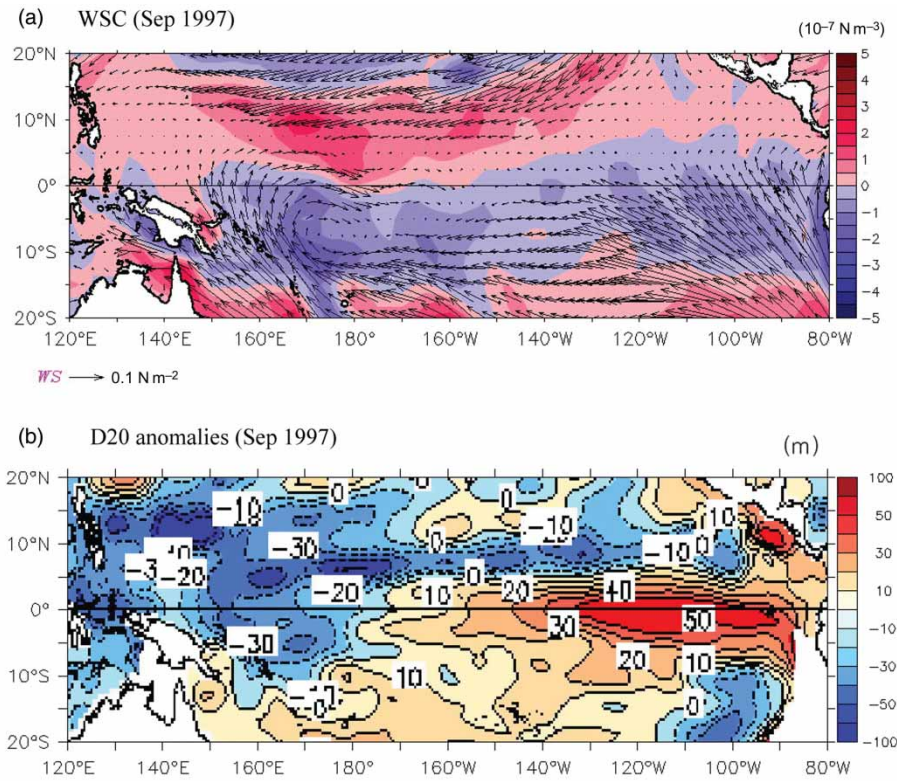


Fig. 9 (a) Wind stress curl pattern and (b) 20°C isotherm depth anomalies in September 1997. The contour interval for the wind stress curl is  $0.5 \times 10^{-7} \text{ N m}^{-3}$  and for the isotherm depth is 10 m.

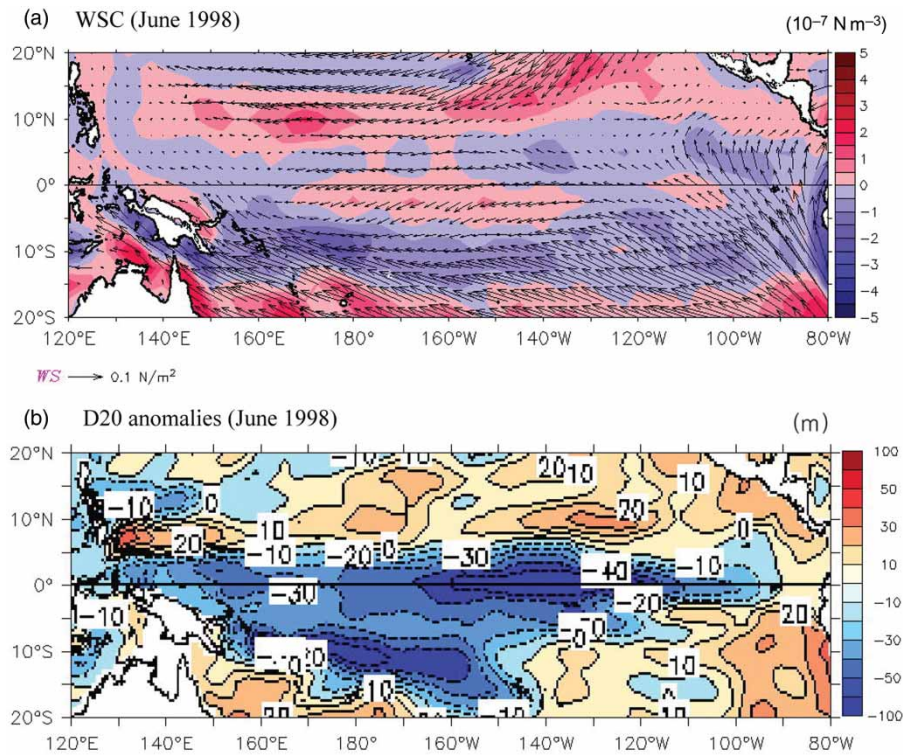


Fig. 10 As in Fig. 9 except for June 1998.

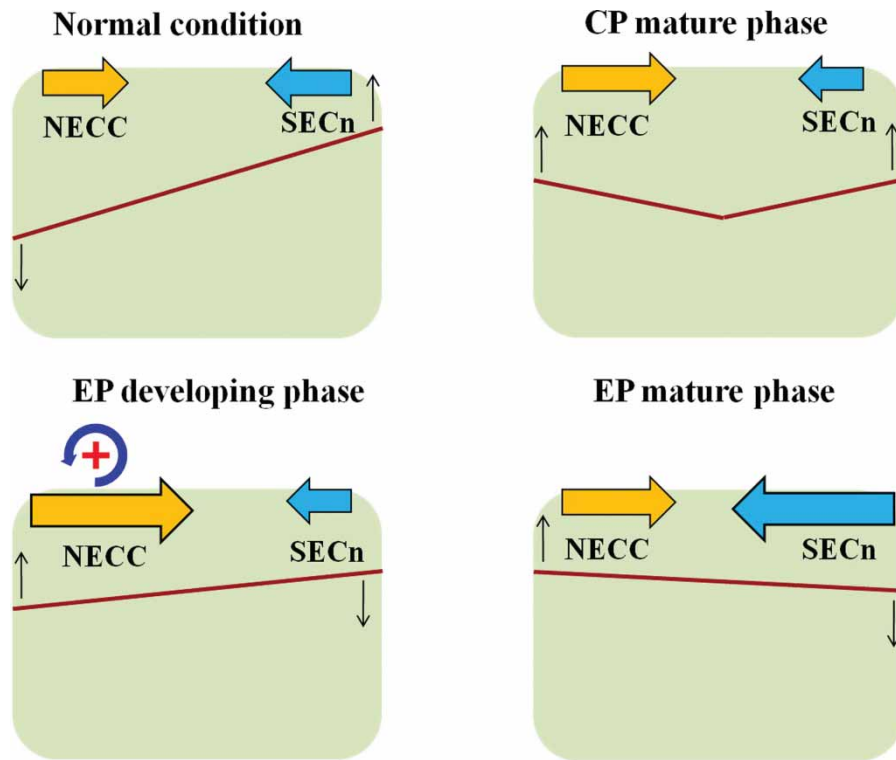


Fig. 11 Schematic diagram illustrating the flow patterns between the eastward NECC and the westward SECn during El Niño evolutionary phases. The coloured arrows indicate the currents, and the solid red line indicates the variation of the thermocline around the equator.

strengthening pattern discussed earlier, demonstrating that the zonal currents intensify significantly during the EP-El Niño compared to the CP-El Niño.

#### d Forcing Mechanism

In this study, we demonstrate that both the SECn and EUC weaken, whereas the NECC becomes stronger during the CP-El Niño. This finding somehow matches the earlier description for the equatorial current variability during El Niño events. It is important to note that both the SECn and EUC strengthen at the warm peak of the EP-El Niño. Because the EUC shoals toward the sea surface, it merges with the NECC and counteracts the westward SEC around the equator. Thus, the current circulation displays a different pattern than shown in previous studies which indicates that both currents weaken during an El Niño.

The reason for the current variability can be linked to the effects of wind stress curl (WSC). The meridional migration of the positive WSC exhibits a seasonal cycle. We further found that the zero WSC line shifts much further south during the EP-El Niño than during the CP-El Niño. For example, in September 1997, the zero WSC line is situated near the equator (Fig. 9a), which is farther south than during the developing phase of the CP-El Niño (figure not shown). A near-symmetric WSC is shown across the equator with positive values to the north (approximately  $10^{\circ}\text{N}$ ,  $170^{\circ}\text{E}$ ) and negative to the south (approximately  $10^{\circ}\text{S}$ ,  $170^{\circ}\text{E}$ ), both elevating the thermocline (Fig. 9b, the negative value represents

a shallower thermocline). The  $20^{\circ}\text{C}$  isotherm depth (D20) anomalies used in this study are based on the GODAS model assimilation. The D20 is generally situated close to the equatorial thermocline and is often used as a proxy for the thermocline depth (e.g., Ji & Leetmaa, 1997; Kessler, 1990). The raised D20 implies shoaling of the EUC, which is found to merge and intensify the NECC during the mature phase of the EP-El Niño. The large and positive WSC in the northwestern equatorial Pacific Ocean also promotes Ekman pumping in the region, resulting in a thermocline ridge. The ridge causes a meridional sea level gradient, which further intensifies the eastward NECC, especially east of  $120^{\circ}\text{W}$  near the eastern boundary. The strengthening of the NECC lasts almost five months.

In addition to the migration of the WSC pattern, the intensity of the WSC also contributes to the different evolution patterns under the two types of El Niño events. We found that the positive WSC in the northwestern Pacific is much larger in the EP-El Niño than that in the CP-El Niño during the developing phase. The stronger WSC results in large thermocline depth variations during the developing phase of the EP-El Niño. The D20 in the western Pacific Ocean is found to be almost 100 m shallower than in the eastern Pacific Ocean (figure not shown). This east–west D20 gradient fits well with the precondition of the warm water discharge process, according to the recharge–discharge oscillator theory (e.g., Jin, 1997; Wyrski, 1985). Because the subsurface EUC flows mainly along the thermocline, the EP-El Niño with a large east–

west D20 gradient can strengthen the EUC from the developing phase to the mature peak of the EP-El Niño.

The intensification of the surface SEC is different from that of the subsurface current. As the NECC intensifies during the developing phase, it transports surface warm water eastward and accumulates in the eastern Pacific Ocean. The zonal sea level gradient (or westward pressure gradient force) strengthens, which intensifies the surface SEC during the EP-El Niño. In addition to sea level gradient, the intensified trade winds also play a critical role in the SEC intensification. The SECs and SECn merge and flow westward close to the equator during the EP-El Niño (Fig. 4c). From the mature phase to the decaying phase of the EP-El Niño, the easterly trade winds intensify and prevail around 120°W–160°E along the equator. The easterly winds drive the SEC downwind and contribute significantly to its intensification along the equator where the Coriolis force tends to be very weak. On the other hand, the zonal sea level gradient is much weaker during the CP-El Niño, when the easterly trade winds also relax. Thus, the westward SEC weakens during the CP-El Niño.

When evolving into the decaying phase, the WSC pattern migrates even farther northward and far from the equator, and a strong negative WSC (centred at approximately 10°S, 175°E) dominates in the southwestern Pacific Ocean (Fig. 10a). The large and negative WSC elevates the thermocline (or decreases the sea level) in the southwestern Pacific Ocean (Fig. 10b), resulting in meridional pressure gradient anomalies around the equator, which drives a stronger SECC eastward over the approximate region 5°S–15°S, 160°E–150°W. The result shown in this simulation is consistent with that in Zhang, Lin, and Zhang (2007) who conducted several idealized experiments using three ocean–atmosphere general circulation models to investigate the air–sea coupling effects of the surface winds, the Intertropical Convergence Zone (ITCZ) and the SECC.

#### 4 Concluding remarks

The general circulation pattern and seasonal variation of the equatorial Pacific Ocean show up quite realistically in the GODAS assimilation model. The circulation pattern during the CP-El Niño is in good agreement with previous studies showing that both the EUC and SEC weaken, while the NECC becomes stronger. On the other hand, the EP-El Niño exhibits a different circulation pattern. The NECC strengthens from the developing phase until the warm peak, and both the SEC and EUC intensify and counteract each other during the mature phase of the EP-El Niño.

The shifting of the WSC field associated with the thermocline variability is chiefly responsible for the unique current

performance of the EP-El Niño. During the developing phase, the strong positive WSC in the northwestern Pacific Ocean induces an elevated thermocline, forming a meridional sea level gradient, and intensifies the NECC. At the warm peak of the EP-El Niño, the easterly trade winds intensify and continue for nearly seven months. The easterly winds, together with the sharp westward pressure gradient force, are responsible for the strengthening of the surface SEC. Figure 11 is a schematic diagram illustrating the flow patterns between the eastward NECC and the westward SECn during El Niño evolutionary phases. The coloured arrows indicate the currents, and the red line indicates the thermocline variation. In a normal year, the westward SECn dominates at the equator and raises the thermocline in the eastern Pacific Ocean. During the CP-El Niño, the SECn weakens whereas the eastward NECC strengthens slightly. During the developing phase of the EP-El Niño, the NECC intensifies significantly (especially as it flows towards the eastern Pacific), which is mainly associated with the positive WSC in the northwestern Pacific Ocean. The SECn is still weak. At the warm peak of the EP-El Niño, the SECn strengthens on the equator. One of the most striking features is the eastward current (from the merging of the NECC with the shoaling EUC) interacting with the westward current (the two branches of the SEC) to form a unique EP-El Niño circulation pattern.

As it moves into the decaying phase, the large negative WSC in the southwestern Pacific Ocean raises the thermocline through Ekman pumping, resulting in a meridional sea level gradient. Hence, the SECC intensifies, inducing an air–sea interaction and may affect the termination of the EP-El Niño. The present study suggests that the ocean–atmosphere interaction plays an important role in the strengthening of the EP-El Niño, which updates some recent studies showing that the EP-El Niño is mostly produced by basin-wide thermocline variations (e.g., Kao & Yu, 2009; Kug et al., 2009; Yu & Kim, 2010).

#### Acknowledgements

The authors would like to thank the editor, Dr. Guoqi Han, and the anonymous reviewers for their careful review of the manuscript and detailed suggestions for its improvement. The authors are grateful to Drs Tzu-Ling Chiang, Cheng-Ta Chen, Lie-Yauw Oey and Chih-Chen Hong for useful communications on the topic and to D. J. Shea and colleagues from NCAR for assistance in processing the GODAS output. This research was supported by the National Science Council, Taiwan, ROC, under grants NSC 100-2119-M-001-029-MY5 and NSC 101-2917-I-003-002.

#### References

- Ashok, K., Behera, S., Rao, A. S., Weng, H., & Yamagata, T. (2007). El Niño Modoki and its teleconnection. *Journal of Geophysical Research*, 112, C111007. doi:10.1029/2006JC003798
- Behringer, D., & Xue, Y. (2004). Evaluation of the global ocean data assimilation system at NCEP: The Pacific Ocean. Eighth Symposium on Integrated Observing and Assimilation Systems for Atmosphere, Oceans,

- and Land Surface, AMS 84th Annual Meeting, Washington State Convention and Trade Center, Seattle, Washington, pp. 11–15.
- Bjerknes, J. (1969). Atmospheric teleconnections from the equatorial Pacific. *Monthly Weather Review*, *97*, 163–172.
- Cai, W., & Whetton, P. H. (2000). Evidence for time-varying pattern of greenhouse warming in the Pacific Ocean. *Geophysical Research Letters*, *27*, 2577–2580.
- Delcroix, T., Eldin, G., Radenac, M. H., Toole, J., & Firing, E. (1992). Variations of the western equatorial Pacific Ocean, 1986–1988. *Journal of Geophysical Research*, *97*, 5423–5445.
- Gouriou, Y., & Toole, J. (1993). Mean circulation of the upper layers of the western equatorial Pacific Ocean. *Journal of Geophysical Research*, *98*, 22495–22520.
- Gu, D., & Philander, S. G. H. (1997). Interdecadal climate fluctuations that depend on exchanges between the tropics and the extratropics. *Science*, *275*, 805–807.
- Ji, M., & Leetmaa, A. (1997). Impact of data assimilation on ocean initialization and El Niño prediction. *Monthly Weather Review*, *125*, 742–753.
- Jin, F. (1997). An equatorial ocean recharge paradigm for ENSO. Part I: Conceptual model. *Journal of Atmospheric Science*, *54*, 811–829. doi:10.1175/1520-0469054<0811:AEORPF>2.0.CO;2
- Johnson, G. C., McPhaden, M. J., Rowe, G. D., & McTaggart, K. E. (2000). Upper equatorial Pacific Ocean current and salinity variability during the 1996–1998 El Niño–La Niña cycle. *Journal of Geophysical Research*, *105*, 1037–1053.
- Johnson, G. C., Sloyan, B. M., Kessler, W. S., & McTaggart, K. E. (2002). Direct measurements of upper ocean currents and water properties across the tropical Pacific during the 1990s. *Progress in Oceanography*, *52*, 31–61.
- Kanamitsu, M., Ebisuzaki, W., Woollen, J., Yang, S. K., Hnilo, J. J., Fiorino, M., & Potter, G. L. (2002). NCEP–DOE AMIP–II reanalysis R–2. *Bulletin of the American Meteorological Society*, *83*, 1631–1643.
- Kao, H. Y., & Yu, J. Y. (2009). Contrasting eastern-Pacific and central-Pacific types of ENSO. *Journal of Climate*, *22*, 615–632. doi:10.1175/2008JCLI2309.1
- Keenlyside, N., & Kleeman, R. (2002). Annual cycle of equatorial zonal currents in the Pacific. *Journal of Geophysical Research*, *107*(C8), 3093. doi:10.1029/2000JC000711
- Kessler, W. S. (1990). Observations of long Rossby waves in the northern tropical Pacific. *Journal of Geophysical Research*, *95*(C4), 5183–5217.
- Kug, J. S., Choi, J., An, S. I., Jin, F., & Wittenberg, A. T. (2010). Warm pool and cold tongue El Niño events as simulated by the GFDL 2.1 coupled GCM. *Journal of Climate*, *23*, 1226–1239.
- Kug, J. S., Jin, F., & An, S. I. (2009). Two types of El Niño events: Cold tongue El Niño and warm pool El Niño. *Journal of Climate*, *22*, 1499–1515. doi:10.1175/2008JCLI2624.1
- Li, T., & Philander, S. G. H. (1996). On the annual cycle of the eastern equatorial Pacific. *Journal of Climate*, *9*, 2986–2998.
- Lukas, R. (1986). The termination of the equatorial undercurrent in the eastern Pacific. *Progress in Oceanography*, *16*, 63–90.
- Lukas, R. (2001). Pacific equatorial currents. In J. H. Steele, S. A. Thorpe, & K. A. Turekian (Eds.), *Encyclopedia of ocean sciences* (pp. 2069–2076). London: Academic Press.
- Philander, S. G. H. (1990). *El Niño, La Niña, and the Southern Oscillation*. New York: Academic Press.
- Philander, S. G. H., Yamagata, T., & Pacanowski, R. C. (1984). Unstable air–sea interaction in the Tropics. *Journal of Atmospheric Science*, *41*, 604–613.
- Welch, B. L. (1947). The generalization of “student’s” problem when several different population variances are involved. *Biometrika*, *34*, 28–35.
- Wyrtki, K. (1974). Sea level and the seasonal fluctuations of the equatorial currents in the western Pacific Ocean. *Journal of Physical Oceanography*, *4*, 91–103.
- Wyrtki, K. (1985). Water displacements in the Pacific and the genesis of El Niño cycles. *Journal of Geophysical Research*, *90*, 7129–7132. doi:10.1029/JC090iC04p07129
- Yeh, S. W., Kug, J. S., Dewitte, B., Kwon, M. H., Kirtman, B. P., & Jin, F. (2009). El Niño in a changing climate. *Nature*, *461*, 511–514. doi:10.1038/nature08316
- Yu, J. Y., & Kim, S. T. (2010). Three evolution patterns of central-Pacific El Niño. *Geophysical Research Letters*, *37*, L08706. doi:10.1029/2010GL042810
- Yu, X., & McPhaden, M. J. (1999). Dynamical analysis of seasonal and inter-annual variability in the equatorial Pacific. *Journal of Physical Oceanography*, *29*, 2350–2369.
- Zhang, X., Lin, W., & Zhang, M. (2007). Toward understanding the double Intertropical Convergence Zone pathology in coupled ocean–atmosphere general circulation models. *Journal of Geophysical Research*, *112*, D12102. doi:10.1029/2006JD007878